Decoupled Active and Reactive Power Control for Large-Scale Grid-Connected Photovoltaic Systems Using Cascaded Modular Multilevel Converters

Liming Liu, *Senior Member, IEEE*, Hui Li, *Senior Member, IEEE*, Yaosuo Xue, *Senior Member, IEEE*, and Wenxin Liu, *Member, IEEE*

***Abstract*—Large-scale grid-connected photovoltaic (PV) systems significantly contribute to worldwide renewable energy growth and penetration, which has inspired the application of cascaded modular multilevel converters due to their unique features such as modular structures, enhanced energy harvesting capability, scalability and so on. However, power distribution and control in the cascaded PV system faces tough challenge on output voltage overmodulation when considering the varied and nonuniform solar energy on segmented PV arrays. This paper addresses this issue and proposes a decoupled active and reactive power control strategy to enhance system operation performance. The relationship between output voltage components of each module and power generation is analyzed with the help of a newly derived vector diagram which illustrates the proposed power distribution principle. On top of this, an effective control system including active and reactive components extraction, voltage distribution and synthesization, is developed to achieve independent active and reactive power distribution and mitigate the aforementioned issue. Finally, a 3-MW, 12-kV PV system with the proposed control strategy is modeled and simulated in MATLAB and PSIM cosimulation platform. A downscaled PV system including two cascaded 5-kW converters with proposed control strategy is also implemented in the laboratory. Simulation and experimental results are provided to demonstrate the effectiveness of the proposed control strategy for large-scale grid-connected cascaded PV systems.**

***Index Terms*—Cascaded PV system, decoupled active and reactive power control, voltage distribution.**

I. Introduction

GLOBAL energy crises and environmental concerns [1]–[3] from conventional fossil fuels have attracted more and more renewable energy developments in the worldwide. Among of these renewable energy, solar energy is much easier to be harvested, converted, and delivered to grid by a variety of power converters [4]–[14]. In particular, large-scale grid-connected photovoltaic (PV) systems play a major role to achieve PV grid parity and have been put forward in high penetration renewable energy systems [15]. As one type of modular multilevel converters, cascaded multilevel converters share many merits of modular multilevel converters, e.g., lower electromagnetic interference, low device rating, improved harmonic spectra, modularity, etc., but also is very promising for the large-scale PV system due to its unique advantages such as independent maximum power point tracking (MPPT) for segmented PV arrays, high ac voltage capability, etc. [11]–[14].

However, cascaded multilevel converters in PV systems are different from their some successful application such as medium voltage motor drive, static synchronous compensator (STATCOM), harmonic compensator, solid state transformer, which are connected with symmetrical segmented dc sources [16]–[22]. PV systems with cascaded multilevel converters have to face tough challenges considering solar power variability and mismatch of maximum power point from each converter module due to manufacturing tolerances, partial shading, dirt, thermal gradients, etc. In a cascaded PV system, the total ac output voltage is synthesized by the output voltage from each converter module in one phase leg, which must fulfill grid codes or requirements. Because same grid current flows through ac side of each converter module, active power mismatch will result in unsymmetrical ac output voltage of these modules [14]. The converter module with higher active power generation will carry more portion of the whole ac output voltage, which may cause overmodulation and degrade power quality if proper control system is not embedded into the cascaded PV system.

Several control strategies have been proposed for the cascaded PV system with direct connection between individual inverter module and segmented PV arrays [23]–[27]. But they did not consider the fact that PV arrays cannot be directly connected to the individual inverter module in high-voltage large-scale PV system application due to the PV insulation and leakage current issues. Even if there are low-frequency medium-voltage transformers between the PV converters and grid, there are still complicated ground leakage current loops among the PV converter modules [28]. Therefore, those methods in [23]–[27] are not qualified for a practical large-scale grid-connected cascaded PV system. Moreover, reactive power compensation was not achieved in [23]–[26], which largely limits the functions of the

Manuscript received September 28, 2013; revised December 22, 2013; accepted January 23, 2014. Date of publication February 6, 2014; date of current version August 26, 2014. Recommended for publication by Associate Editor J. Mahseredjian.

L. Liu is with the ABB Inc., Raleigh, NC 27513 USA (e-mail: limingcaps@gmail.com).

H. Li is with the Department of Electrical and Computer Engineering, College of Engineering, Florida State University, Tallahassee, FL 32310 USA (e-mail: hli@caps.fsu.edu).

Y. Xue is with the Siemens Corporate Research, Princeton, NJ 08540 USA (e-mail: yaosuo.xue@siemens.com).

W. Liu is with the Department of Electrical and Computer Engineering, New Mexico State University, Las Cruces, NM 88003 USA (e-mail: wliu@nmsu.edu).

Color versions of one or more of the figures in this paper are available online at http://ieeexplore.ieee.org.

Digital Object Identifier 10.1109/TPEL.2014.2304966

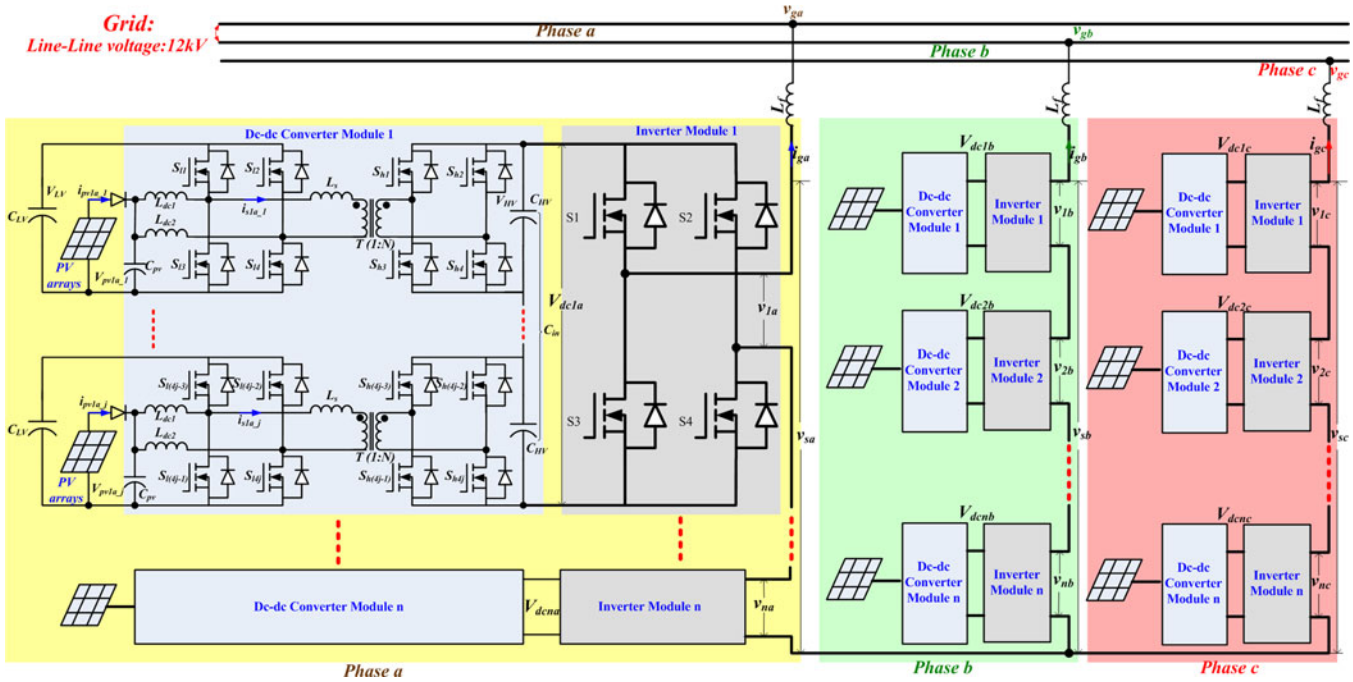

Fig. 1. Proposed grid-connected PV system with cascaded multilevel converters at 3 MW.

cascaded PV system to provide ancillary services. Proper reactive power compensation can significantly improve the system reliability, and in the meantime help the MPPT implementation for the cascaded module under unsymmetrical condition as well as comply with the system voltage requirement simultaneously [29]. A reactive and active power control strategy has been applied in cascaded PV system with isolated dc–dc converters in [30] and [31]. If symmetrical active power comes from each module, active and reactive power can be equally distributed into these modules under traditional power control in [30] and [31]. However, if unsymmetrical active power is generated from these modules, this control strategy will not be able to achieve decoupled active and reactive power control. Reactive power change is along with the active power change at the same direction, which may aggravate output voltage overmodulation during unsymmetrical active power outputs from segmented PV arrays.

In order to solve the aforementioned issues, this paper proposes a large-scale grid-connected cascaded PV system including current-fed dual-active-bridge (CF-DAB) dc–dc converters and cascaded multilevel inverters as shown in Fig. 1. A decouple active and reactive power control system is developed to improve the system operation performance. Reactive power from each PV converter module is synchronously controlled to reduce the overmodulation of PV converter output voltage caused by unsymmetrical active power from PV arrays. In particular, the proposed PV system allows a large low-frequency dc voltage ripple for each PV converter module, which will not affect MPPT achieved by CF-DAB dc–dc converters. As a result, film capacitors can be applied to replace the conventional electrolytic capacitors, thereby enhancing system lifetime.

This paper is organized as follows: a two-stage large-scale grid-connected cascaded PV system topology and corresponding power flow distribution are first introduced in Section II. A vector method is derived to help illustrate the active and reactive power distribution principle between the cascaded PV inverter modules. In Section III, a comprehensive control system with CF-DAB dc–dc converters control and cascaded multilevel inverter control is developed. The decoupled active and reactive power control including active and reactive components extraction, voltage distribution and synthesization, is executed in multilevel inverter control system to achieve independent active and reactive power distribution. A three-phase 3-MW/12-kV PV system including 12 cascaded PV inverter modules with the proposed decoupled active and reactive power control strategy is modeled in MATLAB/Simulink and PSIM cosimulation platform. A downscaled PV system prototype including two cascaded 5-kW inverter modules has also been built in the laboratory. Simulation and experiment results are presented to verify the validity of the proposed control strategy in Sections IV and V. Finally, conclusions are presented in Section VI.

II. System Configuration and Power Flow Analysis

A. System Configuration

The proposed large-scale grid-connected PV system is presented in Fig. 1, which demonstrates a three-phase two-stage power conversion system. It includes n cascaded multilevel inverter modules for each phase, where each inverter module is connected to j cascaded CF-DAB dc–dc converter modules with high voltage insulation [32]. This configuration features many impressive advantages comparing with traditional PV systems with line-frequency transformer. The cascaded multilevel inverters are directly connected to the grid without big line-frequency transformer, and the synthesized output voltage from cascaded modules facilitates to be extended to meet high grid voltage

TABLE I
SYSTEM CIRCUIT PARAMETERS IN SIMULATION

Parameters		Symbol	Value
PV inverter modules in each phase	Number	n	4
	DC Capacitor voltage	V_{dcki} (k=1,2...n; i=a,b,c)	3000 V
	DC Capacitor size	C_{in}	400 uF
	Filter inductor	L_f	0.8 mH
	Switching frequency	f_{SW_AC}	5 kHz
CF-DAB DC-DC converter module	Number	j	5
	Capacitor voltage in low voltage capacitor	V_{LV}	300V
	Capacitor voltage in low voltage capacitor	V_{HV}	600V
	Transformer turn ratio	N	2
	PV arrays output voltage	V_{pvki_r} (k=1,2...n; i=a,b,c ; r=1,2...j)	100 V - 200 V
	Leakage inductor	L_s	2.5 μH
	DC inductor value	L_{dc1}, L_{dc2}	12.5 μH
	Capacitor in high voltage side	C_{HV}	2 mF
	Capacitor in low voltage side	C_{LV}	300 uF
	PV arrays output capacitor	C_{PV}	100 uF
	Switching frequency	f_{SW_DC}	50 kHz
Grid (three phase)	Rated real power	P_g	3 MW
	Rated reactive power	Q_g	1.5 MVAR
	Rated RMS line-line voltage	$V_{gL\text{-}L}$	12 kV

requirement due to the modular structure. Each dc–dc converter module is interfaced with segmented PV arrays and therefore the independent MPPT can be achieved to harvest more solar energy. Moreover, it is immune to the double-line-frequency power ripple propagation into PV arrays. Particularly, the ground leakage current and PV insulation issues are effectively suppressed. In addition, flexible control strategies are able to be explored and applied in this topology owing to more control variables and control degree-of-freedom. Although there is no accurate number about the cost benefits comparing with the traditional PV system with line-frequency transformer, it is obvious that the proposed PV system will have lower cost due to high power density and modular structure, which will significantly reduce the cost of the power platform using to install the PV system. This paper is focused on active and reactive power distribution control of the cascaded multilevel inverters in the proposed PV system. The detailed dc–dc converter design has been provided in [32] and will not be repeated in this paper. The selected application is a 3-MW/12-kV PV system in this paper. The n is selected to be 4 considering the tradeoff among the cost, lifetime, passive components, switching devices and frequency selection, and power quality. As a result, power rating of each inverter module is 250 kW. The average dc voltage of each inverter module is 3000 V based on the requirement of inverter output voltage, power devices as well as power quality. The second-order voltage ripple on the dc side is allowed to 20% even higher. Hence, film capacitor with 400 μF, $C_{\rm in}$, is eligible to improve the system lifetime. In addition, the modular structure enables the high-voltage high-frequency SiC power devices for the HVHP PV application. The switching frequency for each power device is 5 kHz. Due to the phase-shift carrier-based phase-width modulation (PWM) control, the PV inverter will generate nine level output voltage and the equivalent output PWM frequency is 40 kHz for each phase. The current ripple of ac inductor is selected to be less than 20% of the rated output current. Therefore, the ac inductor with 0.8 mH, L_f, is acted as the filter. In each dc–dc converter module, $L_{\rm dc1}$ and $L_{\rm dc2}$ are dc inductors, and L_s is leakage inductor. $C_{\rm PV}$ is high-frequency filter capacitor paralleled with PV arrays. High-frequency transformer with turn ration N is connected between low-voltage side (LVS) converter and high-voltage side (HVS) converter. $C_{\rm LV}$ are LVS dc capacitor and $C_{\rm HV}$ are HVS dc capacitor. The detailed parameters have been provided in Table I.

B. Power Flow Analysis

In the cascaded PV system, power distribution between these modules is primarily dominated by their respective ac output voltage because the same grid current flows through these modules in each phase as shown in Fig. 1. Vector diagrams are derived in Fig. 2 to demonstrate the principle of power distribution between four PV inverter modules in phase a. The same analysis can be applied for phases b and c. Considering the relative stability of the grid voltage, v_{ga} is used for the synchronous signal. The α-axis is in phase with grid voltage and the β-axis lags the α-axis by 90° as shown in Fig. 2(a). The *d*-axis is aligned with the grid voltage by the phase-locked loop (PLL) control [8] and the q-axis lags the d-axis by 90°. The components of grid voltage in $\alpha\beta$ stationary frame and *dq* rotating frame can be written in (1) and (2), respectively

$$\begin{cases} v_{ga\_\alpha} = V_{ga}\sin(\omega t) \\ v_{ga\_\beta} = -V_{ga}\cos(\omega t) \end{cases} \tag{1}$$

$$\begin{bmatrix} v_{ga\_d} \\ v_{ga\_q} \end{bmatrix} = \begin{bmatrix} \sin(\omega t) & -\cos(\omega t) \\ \cos(\omega t) & \sin(\omega t) \end{bmatrix} \begin{bmatrix} v_{ga\_\alpha} \\ v_{ga\_\beta} \end{bmatrix} \tag{2}$$

where the ω is the system fundamental frequency, V_{ga} is the amplitude of the grid voltage, $v_{ga\_d} = V_{ga}, v_{gz\_q} = 0$.

The grid current is relatively stable to the grid voltage in steady state. Therefore, the new d-axis (d') can be aligned with the grid current. It is obvious that the d'-axis component of the inverter output voltage $v_{sa\_d'}$ determines the active power

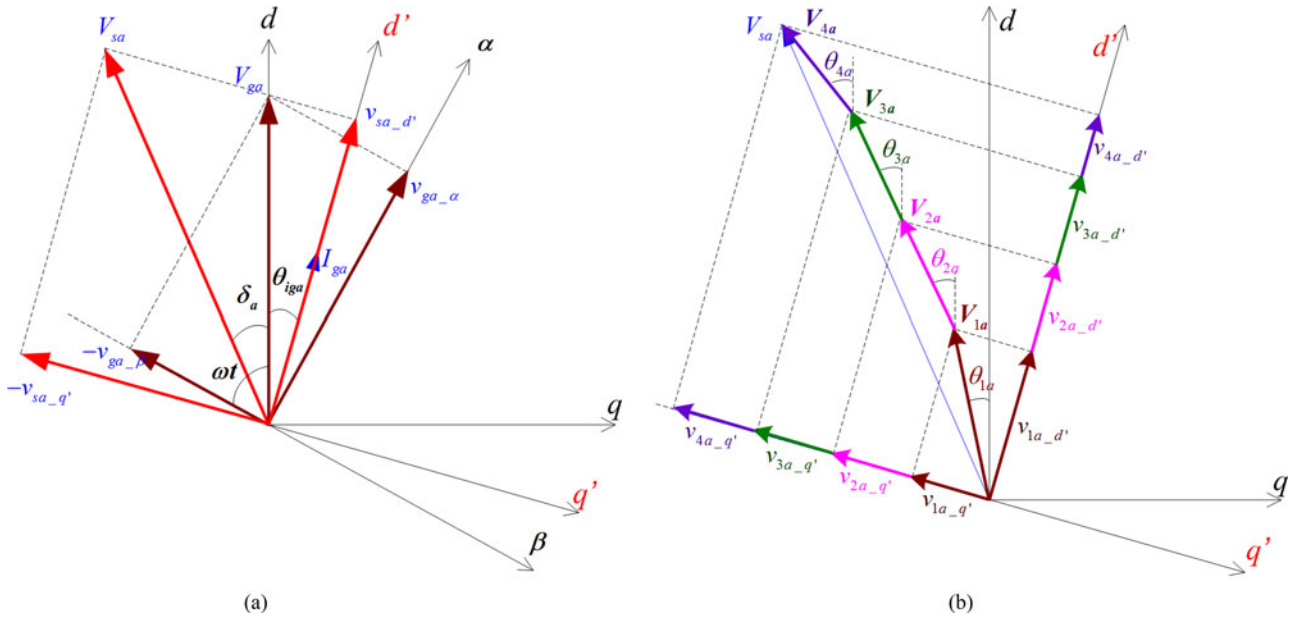

Fig. 2. Vector diagrams showing relation between $\alpha\beta$ frame, dq frame, and $d'q'$ frame. (a) The relationship between the grid current, grid voltage, and inverter output voltage in phase a. (b) The voltage distribution of PV inverter in phase a.

generation, and the q'-axis component $v_{sa\_q'}$ decides the reactive power output. Fig. 2(b) describes clearly the power distribution between four PV inverter modules under different active power generation. The output voltage of the total inverter V_{sa} is synthesized by the four inverter module output voltage with different amplitude and angles. In particular, the $v_{ka\_d'}$ and $v_{ka\_q'}$ ($k = 1, 2,\ldots 4$) can be independently controlled to implement the decoupled active and reactive power control.

III. Control System Design

Fig. 3 shows the proposed control system of the grid-connected cascaded PV converters including CF-DAB dc–dc converters control and cascaded multilevel inverters control in phase a. The same control system can be applied in phases b and c.

A. CF-DAB DC–DC Converters Control

Fig. 3(a) shows the CF-DAB dc–dc converters control for one unit of dc–dc converter module 1 in Fig. 1 [32]. The same control can be used to other units. Due to the dual-active-bridge structure, this control has two degrees of freedom: the duty cycle D and the phase shift angle φ, by which the PV voltage V_{pv1a_1} and LVS dc-link voltage $V_{\rm LV}$ are controlled, respectively. V_{pv1a_1} is directly controlled by the duty cycle D so that it can be well kept at the reference voltage $V^*_{pv1a\_1}$ which is generated from MPPT algorithm [32]. Usually the bandwidth of the duty cycle loop is about several kHz (e.g., 10 kHz in this paper), which is much higher than 120 Hz; thus, the double-frequency component in the LVS or HVS is blocked and high utilization factor of MPPT is reached in the PV side. For simplicity, a simple high bandwidth PI controller is applied. The PV voltage and current are both sensed for the calculation of P_{pv1a_1}, i_{pv1a_1}/v_{pv1a_1}, and $\Delta i_{pv}/\Delta v_{pv}$ which are used in MPPT algorithm. The MPPT algorithm generates a reference voltage $V^*_{pv1a\_1}$ for the PV voltage regulation. Power transferred from LVS to HVS is determined by the phase shift angle φ. By regulating LVS voltage through φ, the power generated from the PV arrays and the power delivered to HVS are matched. To minimize the peak transformer, the LVS dc-link voltage $V_{\rm LV}$ is controlled to follow the reference $\frac{V_{\rm HV}}{N}$, that is HVS voltage divided by turn ratio N, so that they are balanced. Proportional resonant (PR) controller is employed to obtain enough gain at double frequency to ensure the LVS voltage to dynamically follow the reference voltage.

B. Cascaded Multilevel Inverter Control

In the cascaded multilevel converter control showing in Fig. 3(b), active power distribution between cascaded PV converter modules is decided by the individual maximum power available from PV arrays. Considering dc capacitors connected with cascaded multilevel inverter modules have the same capacitance, reactive power from each module can be synchronously controlled to reduce the overmodulation risk regardless of active power change. Therefore, the proposed control strategy can be called decoupled active and reactive power distribution control. The double-loop dq control based on discrete Fourier transform PLL method [8] is applied to achieve the active and reactive power distribution. The unique features of this control strategy is that active and reactive power is decoupled in each module by synchronizing with the grid current as described in Section II, which are not achieved in traditional control methods in [30] and [31]. Due to the same grid current goes through ac side of each module, only grid voltage synchronization is not able to perform the separation of active and reactive power in each module under unsymmetrical active power generation. In the proposed control, individual voltage outer loop controls dc voltage of each inverter module to track the reference $V^*_{\rm dc}$

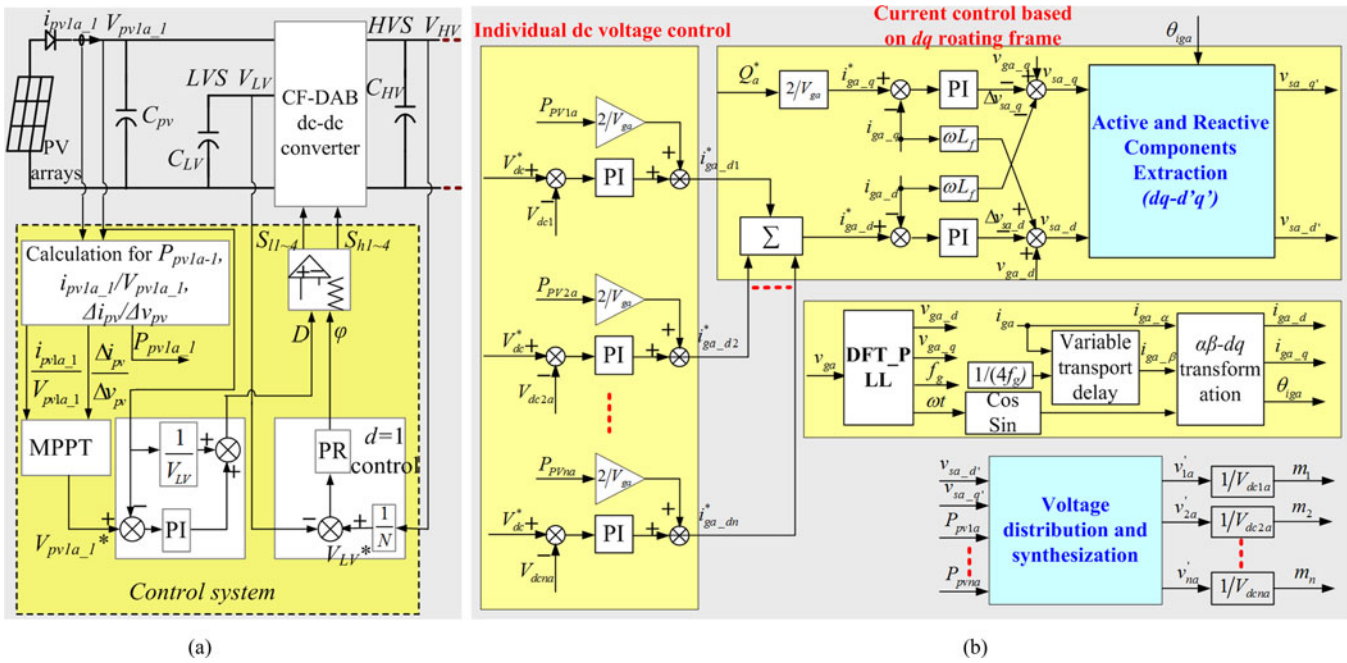

Fig. 3. Proposed control system of the grid-connected cascaded PV converters in phase a. (a) CF-DAB dc–dc converters control of one unit in module 1. (b) Cascaded multilevel inverters control.

by the PI controller. Therefore, the harvested maximum power from j segmented PV arrays with CF-DAB dc–dc converters control can be effectively delivered to grid. Afterward, the maximum power is fed back to reduce the inner loop action. This allows the closed-loop compensators to have smaller gains and hence increased robustness [33]–[35]. The d-axis component command of grid current $i^*_{ga\_d}$ is synthesized by the multiple outputs from the n individual voltage loops. The q-axis component command of grid current $i^*_{ga\_q}$ is obtained based on the desired reactive power Q^*_a. The decoupled current loop controls the dq components of grid current i_{ga_d} and i_{ga_q} to track the references $i^*_{ga\_d}$ and $i^*_{ga\_q}$, and then generates the total output voltage regulation Δv_{sa_d} and Δv_{sa_q}, respectively. The dq components of grid voltage, v_{ga_d} and v_{ga_q}, are feedback to the output voltage to improve the system dynamic performance, respectively [36]. The output voltage signal v_{sa_d} is synthesized by $\Delta v_{sa\_d}, v_{ga\_d}$ and decoupled variable $\omega L_f i_{ga\_q}$. The output voltage signal v_{sa_q} is composed of $\Delta v_{sa\_q} v_{ga\_a}$ and decoupled variable $\omega L_f i_{ga\_d}$. Subsequently, v_{sa_d} and v_{sa_q} are sent to the "active and reactive components extraction" module, which produces the decisive active and reactive components, $v_{sa\_d'}$ and $v_{sa\_q'}$, by synchronizing with i_{ga}. And then the "voltage distribution and synthesization" module divides the $v_{sa\_d'}$ and $v_{sa\_q'}$ into the n cascaded PV inverter modules according to their respective active and reactive power contribution [29].

1) Active and Reactive Components Extraction: The "active and reactive components extraction" module is used to transfer the outputs of inner loops v_{sa_d} and v_{sa_q} in dq frame to $v_{sa_d'}$and $v_{sa\_q'}$ in $d'q'$ frame. The angle of grid current θ_{iga} is the key to achieve the transformation. The grid current i_{ga} can be measured and act as the signal i_{ga_α} in the α-*axis*. The imaginary quadrature signal i_{ga_β} of the grid current can be generated by a variable transport delay block as shown in Fig. 3.

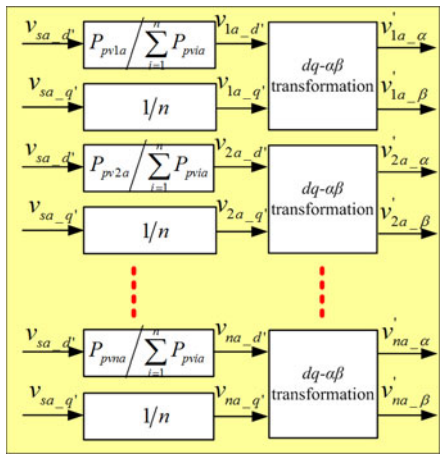

Fig. 4. Proposed voltage distribution and synthesization of the cascaded PV inverters in phase a.

Therefore, θ_{iga} can be obtained based on the dq components of grid current i_{ga_d} and i_{ga_q} by the $\alpha\beta$–dq transformation as follows:

$$\begin{bmatrix} i_{ga\_d} \\ i_{ga\_q} \end{bmatrix} = \begin{bmatrix} \sin\omega t & -\cos\omega t \\ \cos\omega t & \sin\omega t \end{bmatrix} \begin{bmatrix} i_{ga\_\alpha} \\ i_{ga\_\beta} \end{bmatrix} \tag{3}$$

where $\theta_{iga} = tg^{-1}(i_{ga\_q}/i_{ga\_d})$ is the grid current angle.

Accordingly, the desired $v_{sa\_d'}$ and $v_{sa\_q'}$ can be derived by

$$\begin{bmatrix} v_{sa\_d'} \\ v_{sa\_q'} \end{bmatrix} = \begin{bmatrix} \cos\theta_{iga} & \sin\theta_{iga} \\ -\sin\theta_{iga} & \cos\theta_{iga} \end{bmatrix} \begin{bmatrix} v_{sa\_d} \\ v_{sa\_q} \end{bmatrix}. \tag{4}$$

2) Voltage Distribution and Synthesization: The "voltage distribution and synthesization" module as shown in

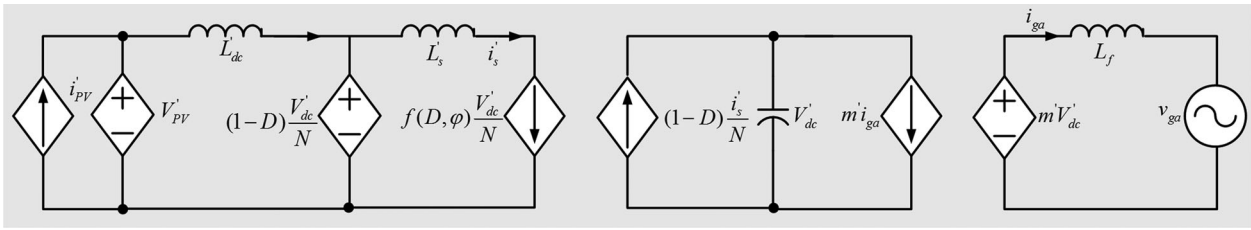

Fig. 5. Equivalent switching function model of the cascaded PV system in phase a.

Fig. 4 is developed to perform the active and reactive power distribution for each module. The active components $v_{ka\_d'}\,(k=1,2,...,n)$ of each module output voltage is determined by their respective active power contribution, which the ratio is $P_{pvka}/\sum_{i=1}^{n} P_{pvia}(k=1,2,...,n)$. The reactive power output from each module is controlled to be the same in order to mitigate output voltage overmodulation caused by unsymmetrical active power from segmented PV arrays [29]. Hence, the corresponding reactive components $v_{ka\_q'}(k=1,2,...,n)$ are distributed with the same ratio $1/n$. Accordingly, the output voltage of each module can be expressed by

$$\begin{bmatrix} v'_{ka\_\alpha} \\ v'_{ka\_\beta} \end{bmatrix} = \begin{bmatrix} \sin(\omega t+\theta_{iga}) & \cos(\omega t+\theta_{iga}) \\ -\cos(\omega t+\theta_{iga}) & \sin(\omega t+\theta_{iga}) \end{bmatrix} \begin{bmatrix} v_{ka\_d'} \\ v_{ka\_q'} \end{bmatrix} \quad (k=1,2,...,n) \tag{5}$$

where $v'_{ka}=v'_{ka\_\alpha}$ is the desired output voltage of each module, v'_{ka_β} is the imaginary quadrature signal with v'_{ka} and can be ignored in this control system.

Therefore, the modulation index of respective output voltage can be obtained by $m_k=\frac{v'_{ka}}{V_{\mathrm{dc}ka}}$ as shown in Fig. 3(b). As a result, the active and reactive power can be properly distributed in each module, which achieves the MPPT and augments the security and stability of the cascaded PV system operation simultaneously.

IV. Simulation Verification

The large-scale grid-connected cascaded PV system with the proposed control strategy is first validated in cosimulation platform with PSIM and MATLAB. The equivalent switching function model in phase a is shown in Fig. 5. The same model can be used in phases b and c. Considering the characteristics of PV arrays, the equivalent input current source i'_{PV} and voltage source V'_{PV} are developed in this model. The duty cycle D determines the LVS voltage as shown in Fig. 3(a) and equivalent dc voltage in cascaded inverter side V'_{dc} is controlled to be constant in Fig. 3(b). Therefore, the equivalent voltage source $(1-D)\frac{V'_{\mathrm{dc}}}{N}$ and current source $(1-D)\frac{i'_s}{N}$ can be integrated into this model, which i'_s is the equivalent primary side transformer current and N is the transformer turn ratio. The equivalent dc inductor L'_{dc} is connected between V'_{PV} and $(1-D)\frac{V'_{\mathrm{dc}}}{N}$. The transferred power by CF-DAB dc–dc converters is determined by both D and φ [32]. Accordingly, the equivalent current source $f(D,\varphi)\frac{i'_s}{N}$ can be obtained and connected with voltage source $(1-D)\frac{V'_{\mathrm{dc}}}{N}$ by equivalent leakage inductor L'_s, which $f(D,\varphi)$ can be derived from [32, (7) and (8)]. The equivalent inverter output $m'V'_{\mathrm{dc}}$ is connected with grid voltage source v_{ga} by grid inductor L_f. The equivalent current source $m'i_{ga}$ is integrated in the middle circuit of this model. The key circuit parameters in simulation are listed in Table I. In this simulation, the fixed simulation step is set to be 1 μs considering the synchronization between simulation points and switching instant [37]. The settling time is about 0.04 s as shown in Figs. 6 and 7.

In this paper, the reactive power injection into grid (inductive reactive power) is defined as negative and reactive power absorption from grid (capacitive reactive power) is defined as positive. The active power injection into grid is defined as positive and active power absorption from grid is defined as negative. Figs. 6 and 7 show the system performance in phase a with traditional control strategy in [30] and [31] and with the proposed control strategy in Fig. 3 under different solar irradiation, respectively. In traditional control strategy, the v_{sa_d} and v_{sa_q} in Fig. 3 are divided by the module number, respectively, and equally distributed in the four cascaded inverter modules in phase a. It does not consider the coupling between active power and reactive power. As a result, the unsymmetrical active power from these modules will affect the reactive power distribution between these modules. The module with high active power generation is required to provide high reactive power, which will cause output voltage overmodulation of this module. However, the proposed decouple active and reactive power control strategy solve the aforementioned issue. v_{sa_d} and v_{sa_q} are reallocated based on the respective active power contribution of these modules. The equivalent reactive power can be generated from these modules regardless of the unsymmetrical active power. The following simulation results provide the verification of the aforementioned analysis. Fig. 6 illustrates the system operation behaviors with traditional control strategy. As shown in Fig. 6(a), the solar irradiation for the four PV inverter modules increases from 200 to 1000 W/m^2 at 0.5 s. The active power to grid, P_{ga}, changes from 0.182 to 1 MW. The reactive power to grid, Q_{ga}, is controlled to be –0.5 MVAR. At 1 s, the solar irradiation on the third and fourth PV inverter modules decreases to 500 W/m^2. Therefore, the active power from them, P_{out_3a} and P_{out_4a}, decreases from 0.25 to 0.12 MW. Accordingly, the reactive power from them, Q_{out_3a} and Q_{out_4a}, decreases from -0.125 MVAR to -0.085 MVAR. In this case, the unsymmetrical active power generation may result in the output voltage overmodulation of the first and second inverter modules because

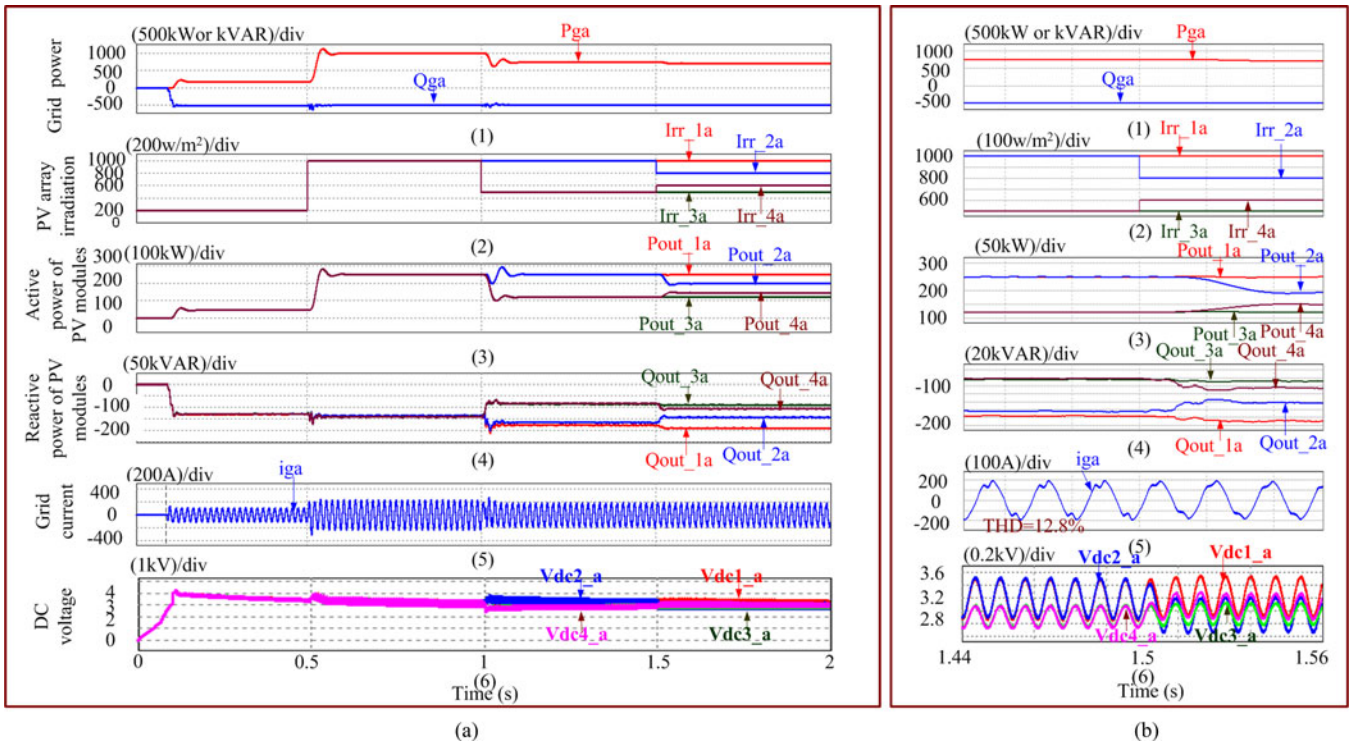

Fig. 6. Simulation results of PV system with traditional active and reactive power control in phase a. (a) Power distribution. (b) Zoomed waveforms at 1.5 s.

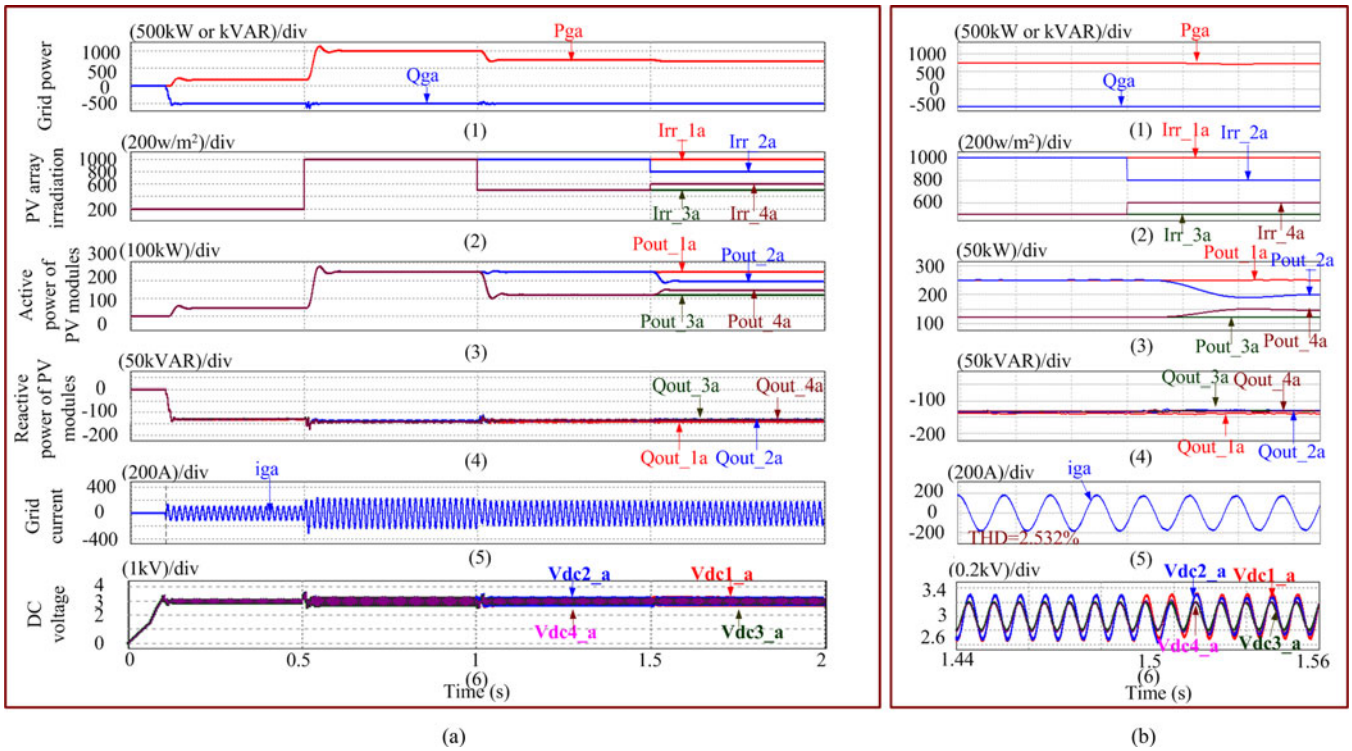

Fig. 7. Simulation results of PV system with decoupled active and reactive power control in phase a. (a) Power distribution. (b) Zoomed waveforms at 1.5 s.

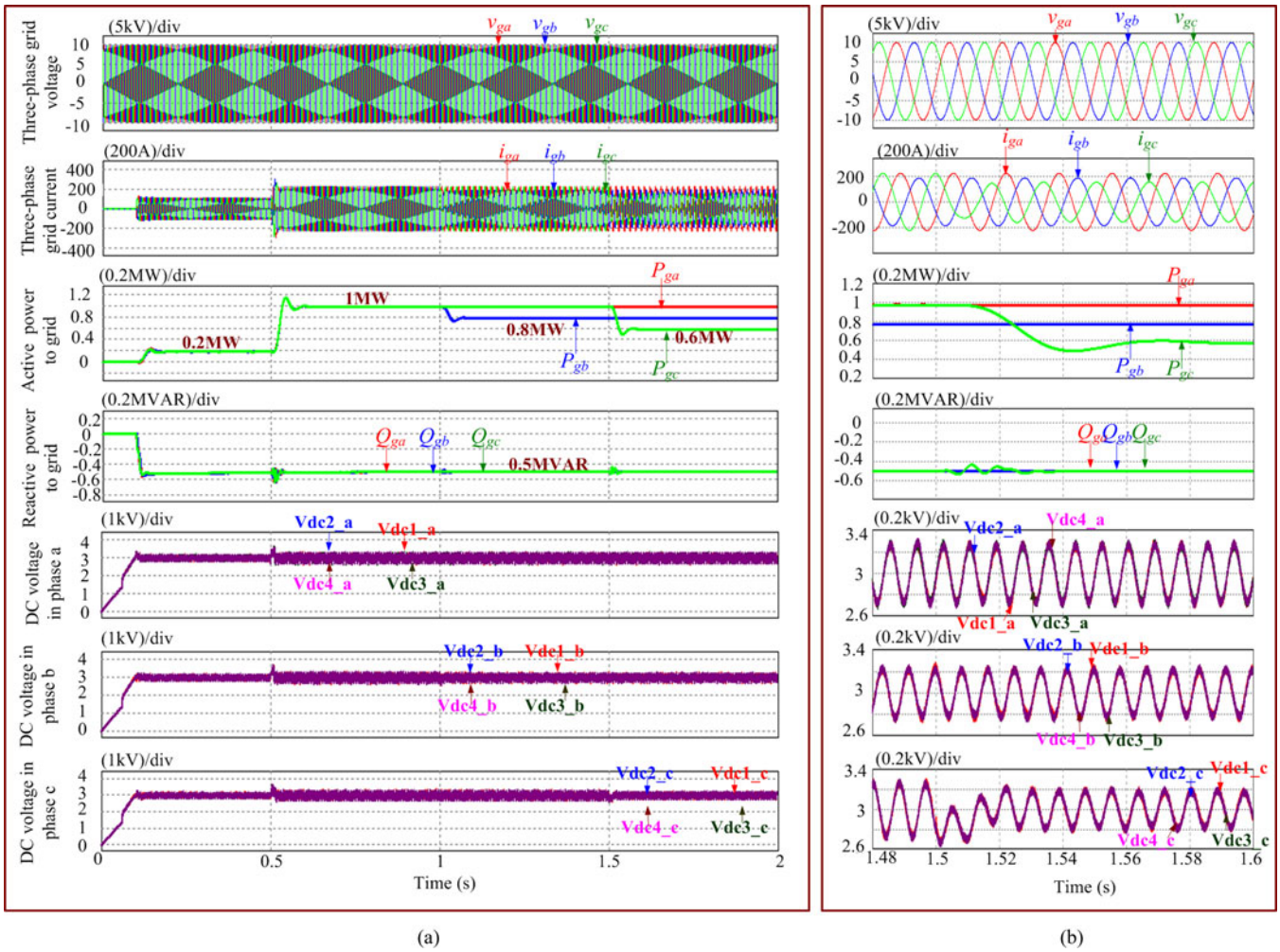

Fig. 8. Simulation results of PV system with the proposed control in three phase. (a) Power distribution. (b) Zoomed waveforms during power transient at 1.5 s.

they will be charged with the more voltage output to meet the system stability. On the other hand, the reactive power from the first and second PV inverter modules, $Q_{\text{out\_1}a}$ and $Q_{\text{out\_2}a}$, increases from -0.125 MVAR to -0.165 MVAR to keep the Q_g to be constant. The increasing burden of reactive power generation exacerbates the output voltage overmodulation from the first and second inverter modules resulting in serious grid current distortion as shown in Fig. 6(b). The total harmonic distortion (THD) of grid current i_{ga} is 12.8%. After 1.5, the solar irradiation for the second–fourth PV inverter modules changes to 800, 600, and 500 W/m^2, respectively. The reactive power changes along with the active power in the same direction. The grid current quality is still poor. The dc voltages on the four modules, $V_{\text{dc\_1}a}$ –$V_{\text{dc\_4}a}$, have poor dynamic performance and deviate from the desired voltage.

Under the same conditions, the proposed control strategy can improve the system operation performance as shown in Fig. 7(a). The active and reactive power can be independently controlled. Although the solar irradiation on first and second inverter modules is different from one on third and fourth inverter modules after 1 s, the reactive power from them is controlled to be symmetrical. By this proper reactive power distribution, the overmodulation caused by the active power mismatch is eliminated. Even when different active power is generated from the four inverter modules after 1.5 s, the effective reactive power compensation can ensure the system with good power quality and stability as shown in Fig. 7(b). It can be seen that THD of i_{ga} is only 2.532%. The dc voltages on the four modules, $V_{\text{dc\_1}a}$ –$V_{\text{dc\_4}a}$, have good dynamic performance and are controlled to vary with 20% rated voltage but do not affect power quality.

Fig. 8(a) shows the simulation results of three-phase cascaded PV system with the proposed control strategy. The solar irradiation for PV inverter modules changes from 200 to 1000 W/m^2 at 0.5 s. The total active power to grid, P_g, increases from 0.6 to 3 MW. The total reactive power to grid, Q_g, is controlled to be -1.5 MVAR. At 1 s, solar irradiation appears on these PV inverter modules in phase b is different from ones in phases a and c. Therefore, different active power is generated from three phase. At 1.5 s, different solar irradiations in the three-phase result in different active powers, P_{ga}, P_{gb}, and P_{gc}, with 1, 0.8, and 0.6 MW, respectively. Thanks to this effective control strategy, the reactive power in the three phase, Q_{ga}, Q_{gb}, and Q_{gc}, can be controlled to be same with 0.5 MVAR. In this

TABLE II
SYSTEM CIRCUIT PARAMETERS IN EXPERIMENT

Parameters		Symbol	Value
PV inverter modules in each phase	Number	n	2
	Capacitor Voltage	V_{dcj} $(j=1,2...n)$	100 V
	Capacitor size	C_{in}	400 uF
	Filter Inductor	L_f	2 mH
	Switching frequency	f_{SW}	10 kHz
Grid (each phase)	Rated real power	P_g	10 kW
	Rated reactive power	Q_g	10 kVAR
	Rated phase-ground voltage (RMS)	v_g	120 V

case, although the grid currents are unbalanced, this system still has good power quality as shown in Fig. 8(b). The dc voltages on these modules, $V_{\mathrm{dc\_1}i}$ –$V_{\mathrm{dc\_4}i}$ ($I = a, b, c$), have good dynamic performance and are controlled to vary with 20% rated voltage.

V. EXPERIMENTAL RESULTS

A downscaled PV system prototype including two cascaded 5-kW PV converter modules with SiC MOSFETs in phase a has been built in the laboratory as shown in Fig. 9. The proposed control strategy is implemented in DSP and FPGA cocontrol platform. The system circuit parameters are modified and listed in Table II considering power loss, actual line impedance, and grid equivalent impedance. The experimental results at 1.1 kVA have been recorded by Yokogawa scopecorder DL750 and carried out to demonstrate the performance of the proposed control system.

Fig. 10 indicates active power distribution, reactive power distribution, grid voltage and current, and frequency spectrum with traditional proposed control strategy [30], [31], respectively. In the initial stage, two PV inverter modules generate the same active power, $P_{pv1} = P_{pv2} = 100$ W, and 150 W active power considering the loss is delivered to grid as shown in Fig. 10(a). The reactive power injected to grid Q_g is 740 VAR, which is less than the sum of Q_{pv1} and Q_{pv2} due to the reactive power loss on output filter and grid impedance as shown in Fig. 10(b). Subsequently, P_g increases from 150 to 770 W and Q_g varies slightly with the grid voltage change. The active and reactive power ratio of two modules is both 0.5:0.5. Afterward, the active power P_{pv1} from first module increases from 412.5 to 490 W and active power P_{pv2} generated by second module decreases from 412.5 to 330 W. Accordingly, the reactive power ratio of two modules changes from 0.5:0.5 to 0.6:0.4 with the active power change at the same direction, which causes the output overmodulation of first PV inverter module. As a result, the grid current i_g is distorted as shown in Fig. 10(c). Finally, P_{pv1} decreases from 490 to 330 W and P_{pv2} increases from 330 to 490 W. Q_{pv1} decreases from 600 to 400 VAR and Q_{pv2} increases from 600 to 400 W. The frequency spectrum of i_g is analyzed under symmetrical and unsymmetrical power distribution. It can be seen from Fig. 10(d) that THD is 8.61% without the proposed control strategy under unsymmetrical power distribution.

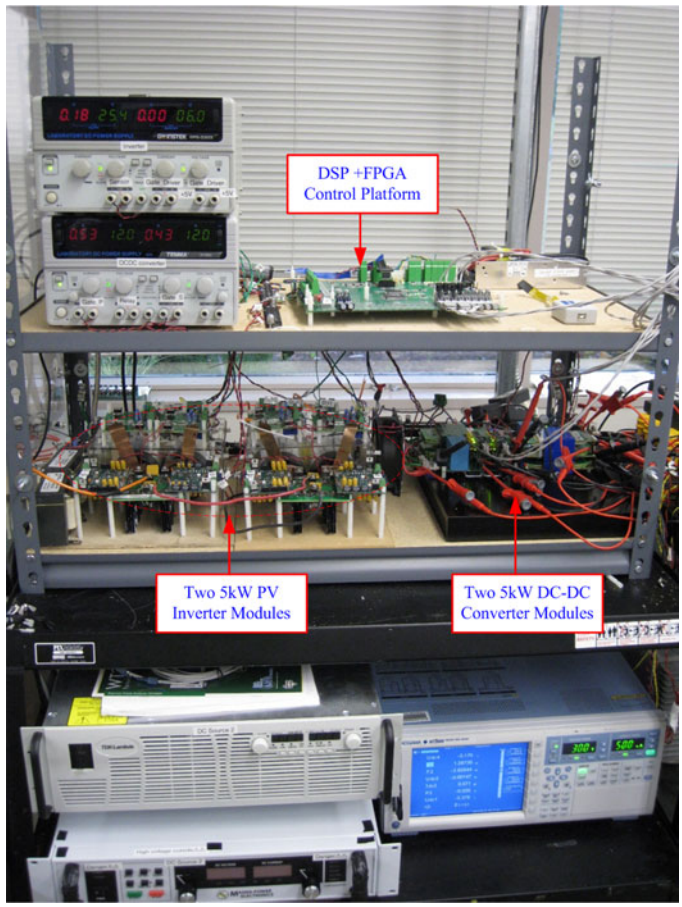

Fig. 9. Laboratorial PV system hardware prototype including two cascaded 5-kW PV converter modules.

Fig. 11 presents active power distribution, reactive power distribution, and grid voltage and current with the proposed control strategy, respectively. Similarly, P_g increases from 150 to 770 W at point 1. The active power from two modules is equalized before point 2 as shown in Fig. 11(a). And then the active power distribution ratio of two modules is 0.6:0.4. After point 3, the ratio changes to 0.4:0.6. During the active power change, the

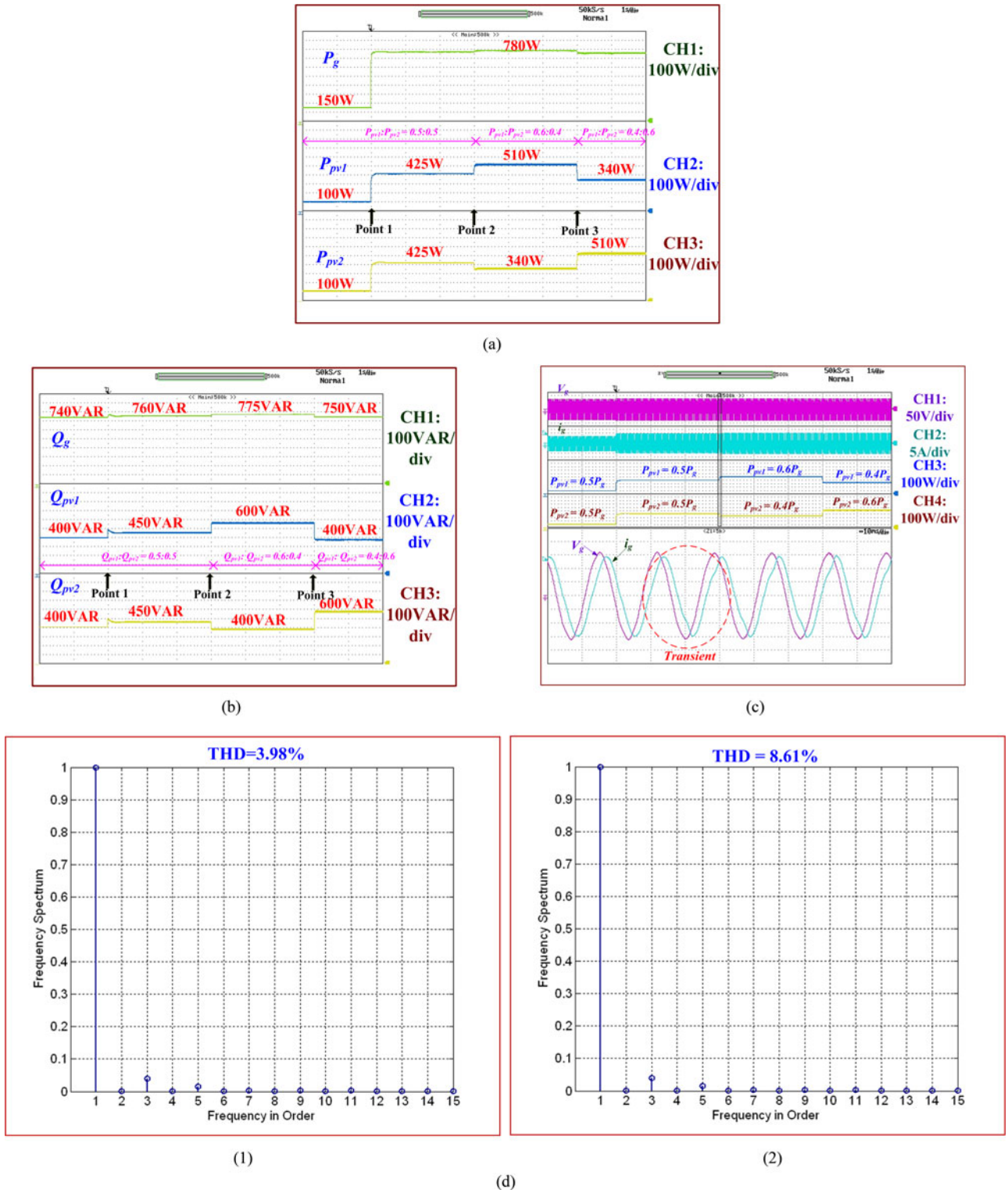

Fig. 10. Experimental results with traditional control strategy. (a) Active power distribution. (b) Reactive power distribution. (c) Grid voltage and current. (d) Frequency spectrum analysis—(1) symmetrical power distribution and (2) unsymmetrical power distribution.

equivalent reactive power is always distributed between the two modules as shown in Fig. 11(b). Because of active and reactive power loss, the sum of P_{PV1} and P_{PV2} is more than P_g, and the sum of Q_{PV1} and Q_{PV2} is greater than Q_g. The grid voltage and current waveform during different active power distribution ratios are illustrated in Fig. 11(c). It can be seen that the grid current has good quality during different scenarios with the proposed control strategy. Furthermore, THD are the same regardless of the unsymmetrical active power distribution, which are only 3.98%.

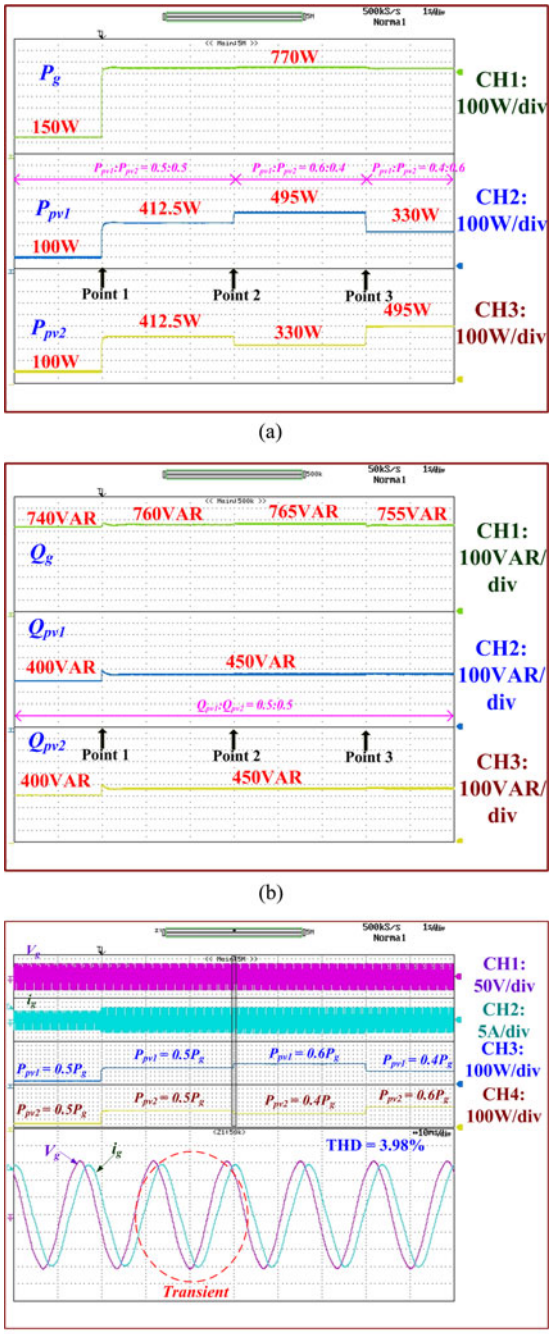

Fig. 11. Experimental results with the proposed control strategy. (a) Active power distribution. (b) Reactive power distribution. (c) Grid voltage and current.

VI. Conclusion

This paper addressed the active and reactive power distribution among cascaded PV inverter modules and their impacts on power quality and system stability for the large-scale grid-connected cascaded PV system. The output voltage for each module was separated based on grid current synchronization to achieve independent active and reactive power distribution. A decoupled active and reactive power control strategy was developed to enhance system operation performance. The proposed control strategy enabled the cascaded PV inverter modules to adequately embody their respective reactive power compensation capability regardless of their active power generation. Moreover, it was demonstrated that the risk of overmodulation of the output voltage from the cascaded PV inverter modules can be effectively reduced, which improves system power quality and stability. Correspondingly, the simulation and experimental results confirmed the validity of the proposed control strategy.

References

[1] Y. Bo, L. Wuhua, Z. Yi, and H. Xiangning, "Design and analysis of a grid connected photovoltaic power system," *IEEE Trans. Power Electron.*, vol. 25, no. 4, pp. 992–1000, Apr. 2010.

[2] J. Ebrahimi, E. Babaei, and G. B. Gharehpetian, "A new topology of cascaded multilevel converters with reduced number of components for high-voltage applications," *IEEE Trans. Power Electron.*, vol. 26, no. 11, pp. 3109–3118, Nov. 2011.

[3] L. Nousiainen and J. Puukko, "Photovoltaic generator as an input source for power electronic converters," *IEEE Trans. Power Electron.*, vol. 28, no. 6, pp. 3028–3037, Jun. 2013.

[4] D. Meneses, F. Blaabjery, O. Garcia, and J. A. Cobos, "Review and comparison of step-up transformerless topologies for photovoltaic AC-module application," *IEEE Trans. Power Electron.*, vol. 28, no. 6, pp. 2649–2663, Jun. 2013.

[5] S. Kjaer, J. Pedersen, and F. Blaabjerg, "A review of single-phase grid connected inverters for photovoltaic modules," *IEEE Trans. Ind. Appl.*, vol. 41, no. 5, pp. 1292–1306, Sep./Oct. 2005.

[6] J. Mei, B. Xiao, K. Shen, L. M. Tolbert, and J. Y. Zheng, "Modular multilevel inverter with new modulation method and its application to photovoltaic grid-connected generator," *IEEE Trans. Power Electron.*, vol. 28, no. 11, pp. 5063–5073, Nov. 2013.

[7] Y. Zhou, L. Liu, and H. Li, "A high performance photovoltaic module-integrated converter (MIC) based on cascaded quasi-Z-source Inverters (qZSI) using eGaN FETs," *IEEE Trans. Power Electron.*, vol. 28, no. 6, pp. 2727–2738, Jun. 2013.

[8] L. Liu, H. Li, and Y. Zhou, "A cascaded photovoltaic system integrating segmented energy storages with self-regulating power distribution control and wide range reactive power compensation," *IEEE Trans. Power Electron.*, vol. 26, no. 12, pp. 3545–3559, Dec. 2011.

[9] Q. Li and P. Wolfs, "A review of the single phase photovoltaic module integrated converter topologies with three different DC link configurations," *IEEE Trans. Power Electron.*, vol. 23, no. 3, pp. 1320–1333, May 2008.

[10] L. Zhang, K. Sun, Y. Xing, L. Feng, and H. Ge, "A modular grid-connected photovoltaic generation system based on DC bus," *IEEE Trans. Power Electron.*, vol. 26, no. 2, pp. 523–531, Feb. 2011.

[11] L. M. Tolbert and F. Z. Peng, "Multilevel converters as a utility interface for renewable energy systems," in *Proc. IEEE Power Eng. Soc. Summer Meet.*, Seattle, Washington, USA, Jul. 2000, pp. 1271–1274.

[12] M. Malinowski, K. Gopakumar, J. Rodriguez, and M. A. Perez, "A survey on cascaded multilevel inverters," *IEEE Trans. Ind. Electron.*, vol. 57, no. 7, pp. 2197–2206, Jul. 2010.

[13] S. Harb and R. S. Balog, "Reliability of candidate photovoltaic module-integrated-inverter (PV-MII) topologies—A usage model approach," *IEEE Trans. Power Electron.*, vol. 28, no. 6, pp. 3019–3027, Jun. 2013.

[14] L. Liu, H. Li, and Y. Xue, "A coordinated active and reactive power control strategy for grid-connected cascaded photovoltaic (PV) system in high voltage high power applications," in *Proc. IEEE 28th Appl. Power Electron. Conf. Expo.*, Long Beach, CA, USA, Mar. 17–21, 2013, pp. 1301–1308.

[15] P. Denholm and R. Margolis, "Very large-scale deployment of grid-connected solar photovoltaics in the united states: Challenges and opportunities," in *Proc. Nat. Renewable Energy Laboratory Conf. Paper Preprint Solar*, U.S. Department of Energy, 2006.

[16] M. Abolhassani, "Modular multipulse rectifier transformers in symmetrical cascaded H-bridge medium voltage drive," *IEEE Trans. Power Electron.*, vol. 27, no. 2, pp. 698–705, Feb. 2012.

[17] K. Sano and M. Takasaki, "A transformerless D-STATCOM based on a multivoltage cascaded converter requiring no dc source," *IEEE Trans. Power Electron.*, vol. 27, no. 6, pp. 2783–2795, Jun. 2012.

[18] C. D. Townsend, T. J. Summers, J. Vodden, A. J. Watson, R. E. Betz, and J. C. Clare, "Optimization of switching losses and capacitor voltage

ripple using model predictive control of a cascaded H-bridge multilevel StatCom," *IEEE Trans. Power Electron.*, vol. 28, no. 7, pp. 3077–3087, Jul. 2013.
[19] B. Gultekin and M. Ermis, "Cascaded multiulevel converter-based transmission STATCOM: System design methodology and development of a 12 kV ± 12 MVAr power stage," *IEEE Trans. Power Electron.*, vol. 28, no. 11, pp. 4930–4950, Nov. 2013.
[20] T. Zhao, G. Wang, S. Battacharya, and A. Q. Huang, "Voltage and power balance control for a cascaded H-bridge converter-based solid-state transformer," *IEEE Trans. Power Electron.*, vol. 28, no. 4, pp. 1523–1532, Apr. 2013.
[21] X. She, A. Q. Huang, and X. Ni, "Current sensorless power balance strategy for DC/DC converters in a cascaded multilevel converter based solid state transformer," *IEEE Trans. Power Electron.*, vol. 29, no. 1, pp. 17–22, Jan. 2014.
[22] S. Du, J. Liu, and J. Lin, "Hybrid cascaded H-bridge converter for harmonic current compensation," *IEEE Trans. Power Electron.*, vol. 28, no. 5, pp. 2170–2179, May. 2013.
[23] E. Villanueva, P. Correa, J. Rodriguez, and M. Pacas, "Control of a single-phase cascaded h-Bridge multilevel inverter for grid-connected photovoltaic systems," *IEEE Trans. Ind. Electron.*, vol. 56, no. 11, pp. 4399–4406, Sep. 2009.
[24] O. Alonso, P. Sanchis, E. Gubia, and L. Marroyo, "Cascaded H-bridge multilevel converter for grid connected photovoltaic generators with independent maximum power point tracking of each solar array," in *Proc. IEEE 34th Annu. Power Electron. Spec. Conf.*, Jun. 2003, vol. 2, pp. 731–735.
[25] J. Negroni, F. Guinjoan, C. Meza, D. Biel, and P. Sanchis, "Energy sampled data modeling of a cascade H-bridge multilevel converter for grid-connected PV systems," in *Proc. IEEE 10th Int. Power Electron. Congr.*, Oct. 2006, pp. 1–6.
[26] F. C. Cecati and P. Siano, "A multilevel inverter for photovoltaic systems with fuzzy logic control," *IEEE Trans. Ind. Electron.*, vol. 57, no. 12, pp. 4115–4125, Dec. 2010.
[27] M. Rezaei, H. Iman-Eini, and S. Farhangi, "Grid-connected photovoltaic system based on a cascaded H-Bridge inverter," *J. Power Electron.*, vol. 12, no. 4, pp. 578–586, Jul. 2002.
[28] Y. Zhou and H. Li, "Leakage current suppression for PV cascaded multilevel inverter using GaN devices," in *Proc. IEEE 5th Energy Convers. Congr. Expo.*, Denver, Colorado, USA, Sep. 15–19, 2013, pp. 1304–1310.
[29] L. Liu, H. Li, Y. Xue, and W. Liu, "Reactive power compensation and optimization strategy for grid-interactive cascaded photovoltaic systems," accepted by *IEEE Trans. Power Electron.*, 2014.
[30] W. Zhao, H. Choi, G. Konstantinou, M. Ciobotaru, and V. G. Agelidis, "Cascaded H-bridge multilevel converter for large-scale PV grid-integration with isolated dc–dc stage," in *Proc. 3rd Int. Symp. Power Electron. Distrib. Generation Syst.*, Aalborg, Denmark, Jun. 25–28, 2012, pp. 849–856.
[31] H. Choi, W. Zhao, M. Ciobotaru, and V. G. Agelidis, "Large-scale PV system based on the multiphase isolated DC/DC converter," in *Proc. 3rd Int. Symp. Power Electron. Distrib. Generation Syst.*, Aalborg, Denmark, Jun. 25–28, 2012, pp. 801–807.
[32] Y. Shi, L. Liu, H. Li, and Y. Xue, "A single-phase grid-connected PV converter with minimal DC-link capacitor and low-frequency ripple-free maximum power point tracking," in *Proc. IEEE 5th Energy Convers. Congr. Expo.*, Denver, Colorado, USA, Sep. 15–19, 2013, pp. 2385–2390.
[33] M. J. Ryan, R. W. D. Doncker, and R. D. Lorenz, "Decoupled control of a four-leg inverter via a new 4_4 transformation matrix," *IEEE Trans. Power Electron.*, vol. 16, no. 5, pp. 694–701, Sep. 2001.
[34] P. C. Loh, M. J. Newman, D. N. Zmood, and D. G. Holmes, "A comparative analysis of multi-loop voltage regulation strategies for single and three-phase UPS systems," *IEEE Trans. Power Electron.*, vol. 18, no. 5, pp. 1176–1185, Sep. 2003.
[35] P. C. Loh and D. G. Holmes, "Analysis of multiloop control strategies for LC/CL/LCL-filtered voltage-source and current-source inverters," *IEEE Trans. Ind. Appl.*, vol. 41, no. 2, pp. 644–654, Mar./Apr. 2005.
[36] A. Lindberg,"PWM and control of two and three level high power voltage source converters," Licentiate thesis, Royal Inst. of Technology, Stockholm, Sweden, 1995.
[37] H. Jin, "Behavior-mode simulation of power electronic circuits," *IEEE Trans. Power Electron.*, vol. 12, no. 3, pp. 443–452, May 1997.

Liming Liu (M'09–SM'11) received the B.S. and M.S. degrees in electrical engineering from Wuhan University, Hubei, China, in 1998 and 2003, respectively, and the Ph.D. degree in electrical engineering from Huazhong University of Science and Technology, Hubei, China, in 2006.

He joined the Center for Advanced Power Systems, Florida State University, Tallahassee, FL, USA, in 2007, as a Postdoctoral Researcher, where he was an Assistant Scientist from 2008 to 2013. He is currently a Senior Scientist at ABB Inc., Raleigh, NC, USA. His research interests generally include medium/high voltage dc voltage converter, modeling and control of multilevel inverter applications, renewable energy conversion systems, high penetrative grid-interactive photovoltaic system, smart grid, motor drive control with hybrid energy storages, and flexible ac transmission system.

Hui Li (S'97–M'00–SM'01) received the B.S. and M.S. degrees in electrical engineering from Huazhong University of Science and Technology, Hubei, China, in 1992 and 1995, respectively, and the Ph.D. degree in electrical engineering from the University of Tennessee, Knoxville, TN, USA, in 2000.

She is currently a Full Professor in the Electrical and Computer Engineering Department, Florida A&M University—Florida State University college of engineering, Tallahassee, FL, USA. Her research interests include bidirectional dc–dc converters, cascaded multilevel inverters and power electronics application in hybrid electric vehicles.

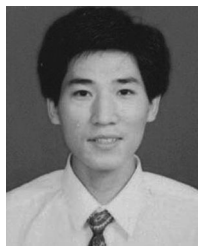

Yaosuo Xue (M'03–SM'12) received the B.Sc. degree in electrical engineering from East China Jiaotong University, Nanchang, China, in 1991, and the M.Sc. degree in electrical engineering from the University of New Brunswick, Fredericton, Canada, in 2004, where he is working toward the Ph.D. degree.

During 2005 to 2006, he was with the Capstone Turbine Corp., CA, USA, as a Lead Power Electronics and Systems Engineer developing advanced microturbine systems. Since 2009, he has been a Research Scientist and currently Research Project Manager at Corporate Technology, Siemens Corporation in Princeton, NJ, USA, where he Cofounded the Siemens Corporate Technology's power electronics research group in USA.

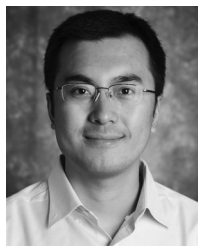

Wenxin Liu (S'01–M'05) received the B.S. and M.S. degrees from Northeastern University, Shenyang, China, in 1996 and 2000, respectively, and the Ph.D. degree in electrical engineering from the Missouri University of Science and Technology (the formerly University of Missouri-Rolla), MO, USA, in 2005.

Then, he worked as an Assistant Scholar Scientist with the Center for Advanced Power Systems of Florida State University until 2009. From 2009 to 2014, he was an Assistant Professor with the Klipsch School of Electrical and Computer Engineering of New Mexico State University, Las Cruces, NM, USA. Currently, he is an Assistant Professor with the Department of Electrical and Computer Engineering of Lehigh University, Bethlehem, PA, USA. His research interests include power systems, power electronics, and controls.